A first principle comparative study of the ionic diffusivity in $LiAlO_2$ and $NaAlO_2$ polymorphs for solid-state battery applications. Electronic Supplementary Information (ESI)

F. Bianchini, H. Fjellvåg, P. Vajeeston
Department of Chemisty
Univeristy of Oslo
Box 1033 Blindern
N-0315 Oslo, Norway

March 7, 2018

Abstract

Lithium aluminates are attracting increasing attention as battery materials. They are typically used for coating of the electrodes. The diffusive properties of the equilibrium tetragonal phase (γ) are well understood from both an experimental and a theoretical perspective, and the major diffusive mechanism is recognised to be vacancy hopping between neighbouring sites. Investigations of this type are however not reported for the other, high pressure $LiAlO_2$ phases. Moreover, the ionic diffusivity of the Na-based aluminates, manifesting a similar polymorphism to $LiAlO_2$, has never been studied using atomistic techniques. In this work, we address these points, by presenting a comparative density functional theory-based study of these materials, describing the structural properties of the various phases, and evaluating the activation energies for single vacancy hops. While $LiAlO_2$ exhibits a poor ionic conductivity due to a significant degree of covalency of the Al–O bonding, orthorhombic β-$NaAlO_2$ exhibits a significantly lower diffusion barrier. This feature cannot be explained only in terms of the larger equilibrium volume, as the same trend is not observed for the high-pressure trigonal α-$LiAlO_2$ and α-$NaAlO_2$. We make here use of various electronic-structure tools to verify the lower degree of covalency of the Na–O bonds. The electron localisation function in particular is shown to be intrinsically correlated to the diffusion pathways of Li and Na ions, and its variation along the path a qualitative measure of ionic conductivity.

1 Structural data

We report here the structural parameters and the atomic coordinates for the optimised structure of the examined $X\mathrm{AlO_2}$ (X = Li, Na) modifications. The data for $\mathrm{LiAlO_2}$ and $\mathrm{NaAlO_2}$ are presented in Table S1 and S3 respectively. The optimised structures have been analysed with the FINDSYM program, referenced in the main text, and the Wyckoff positions have been identified. The standard accuracy of 10^{-3} Å and 10^{-5} Å for atomic positions and lattice parameters have been used. The atomic positions are indicated in fractional coordinates, and the multiplicity of each site is indicated.

Table S1: Lattice parameters and atomic coordinates of the optimised structure of the examined $\mathrm{LiAlO_2}$ modifications. The Wickoff labels and the site multiplicity are indicated. The atomic positions are in fractional coordinates, and the lattice parameters are indicated.

α-$\mathrm{LiAlO_2}$	space group $R\bar{3}m$ (*No* 166)				
$a = b = 2.82624$ Å, $c = 14.36566$ Å, $\alpha = \beta = 90°$, $\gamma = 120°$					
atom	multiplicity	Wyckoff label	x	y	z
Al	3	b	0.00000	0.00000	0.50000
Li	3	a	0.00000	0.00000	0.00000
O	6	c	0.00000	0.00000	0.23826

β-$\mathrm{LiAlO_2}$	space group $Pna2_1$ (*No* 33)				
$a = 5.33654$ Å, $b = 6.36738$ Å, $c = 4.97592$ Å, $\alpha = \beta = \gamma = 90°$					
atom	multiplicity	Wyckoff label	x	y	z
Al	4	a	0.57744	0.37393	0.00212
Li	4	a	0.91630	0.37531	0.50923
O1	4	a	0.55962	0.39627	0.64412
O2	4	a	0.89772	0.35061	0.10013

γ-$\mathrm{LiAlO_2}$	space group $P4_12_12$ (*No* 92)				
$a = b = 5.39390$ Å, $c = 7.01037$ Å, $\alpha = \beta = \gamma = 90°$					
atom	multiplicity	Wyckoff label	x	y	z
Al	4	a	0.67647	0.67647	0.00000
Li	4	a	0.31365	0.31365	0.00000
O	8	b	0.83748	0.79165	0.77179

δ-$\mathrm{LiAlO_2}$	space group $I4_1/amd$ (*No* 144)				
$a = b = 3.89456$ Å, $c = 8.41196$ Å, $\alpha = \beta = \gamma = 90°$					
atom	multiplicity	Wyckoff label	x	y	z
Al	4	a	0.00000	0.75000	0.12500
Li	4	b	0.00000	0.25000	0.37500
O	8	e	0.00000	0.25000	0.10032

Table S2: Lattice parameters and atomic coordinates of the optimised structure of the examined $NaAlO_2$ modifications. The Wickoff labels and the site multiplicity are indicated. The atomic positions are in fractional coordinates, and the lattice parameters are indicated.

α-$NaAlO_2$ space group $R\bar{3}m$ (*No* 166)					
$a = b = 2.89390$ Å, $c = 15.90844$ Å, $\alpha = \beta = 90°$, $\gamma = 120°$					
atom	multiplicity	Wyckoff label	x	y	z
Al	3	b	0.00000	0.00000	0.50000
X	3	a	0.00000	0.00000	0.00000
O	6	c	0.00000	0.00000	0.23041

β-$LiAlO_2$ space group $Pna2_1$ (*No* 33)					
$a = 5.39390$ Å, $b = 7.01037$ Å, $c = 4.97592$ Å, $\alpha = \beta = \gamma = 90°$					
atom	multiplicity	Wyckoff label	x	y	z
Al	4	a	0.56333	0.37428	0.99976
X	4	a	0.92721	0.37747	0.51435
O1	4	a	0.53461	0.41955	0.66854
O2	4	a	0.87779	0.32868	0.07295

γ-$NaAlO_2$ space group $P4_12_12$ (*No* 92)					
$a = b = 5.39390$ Å, $c = 7.01037$ Å, $\alpha = \beta = \gamma = 90°$					
atom	multiplicity	Wyckoff label	x	y	z
Al	4	a	0.69128	0.69128	0.00000
X	4	a	0.29879	0.29879	0.00000
O	8	b	0.86760	0.77152	0.79542

δ-$NaAlO_2$ space group $I4_1/amd$ (*No* 144)					
$a = b = 4.24869$ Å $c = 8.45641$ Å,$\alpha = \beta = \gamma = 90°$					
atom	multiplicity	Wyckoff label	x	y	z
Al	4	a	0.00000	0.75000	0.12500
X	4	b	0.00000	0.25000	0.37500
O	8	e	0.00000	0.25000	0.09100

2 Phonons density of states

The Phonons total density of states are reported in Fig. 2. Calculations for the high pressure δ phase have been neglected, as this phase is energetically unfavourable. In all the reported structure, we observe the lack of imaginary frequencies, characterising these structures as stable. We always observe a shifting in the first peak in the range 0–5 THz between $LiAlO_2$ and $NaAlO_2$, due to the larger mass of Na with respect to Li. The tetrahedral-coordinated phases γ and β are all characterised by a high-frequency double peak in the 22-27 THz region, due to the vibrations of the Al–O bond, as shown in Fig. 3 in the main text. These modes are not present in the high pressure α phase, due to the different coordination geometry. A larger similarity is observed between γ-$NaAlO_2$ and β-$NaAlO_2$, in line with the large overlap between the energy-volume curves observed in Fig. 1 in the main text.

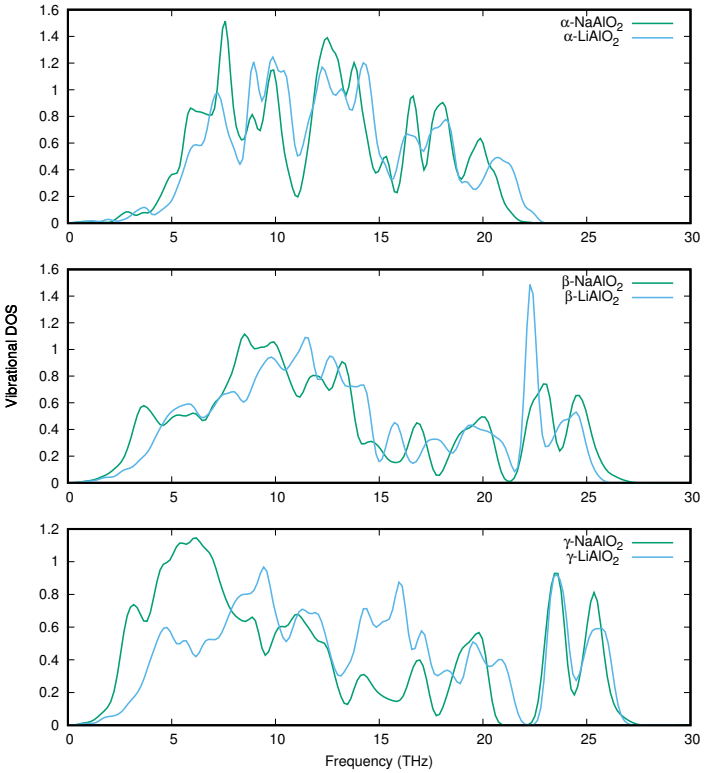

Fig. S1: Phonons density of states for the examined $LiAlO_2$ and $NaAlO_2$ modifications.

3 Activation barriers

We report here the energy curves along the minimum energy path (MEP) for vacancy hopping between neighbouring X sites. The data for $LiAlO_2$ and $NaAlO_2$ are reported in Figure 3, panel (a) and (b) respectively. The nudged elastic band calculation has not been carried out in the case of δ-$NaAlO_2$, as this configurations is very energetically unfavourable, as explained in the main text. The maxima of these curves, are reported in the main text in Table 5, and discussed there. We note that the maximum of each curve corresponds always to image n. 3, due to the intrinsic symmetry of the hops (only equivalent X atoms are present in these structures, as clear from the tables reported in the previous section), and of the usage of the climb-image method.

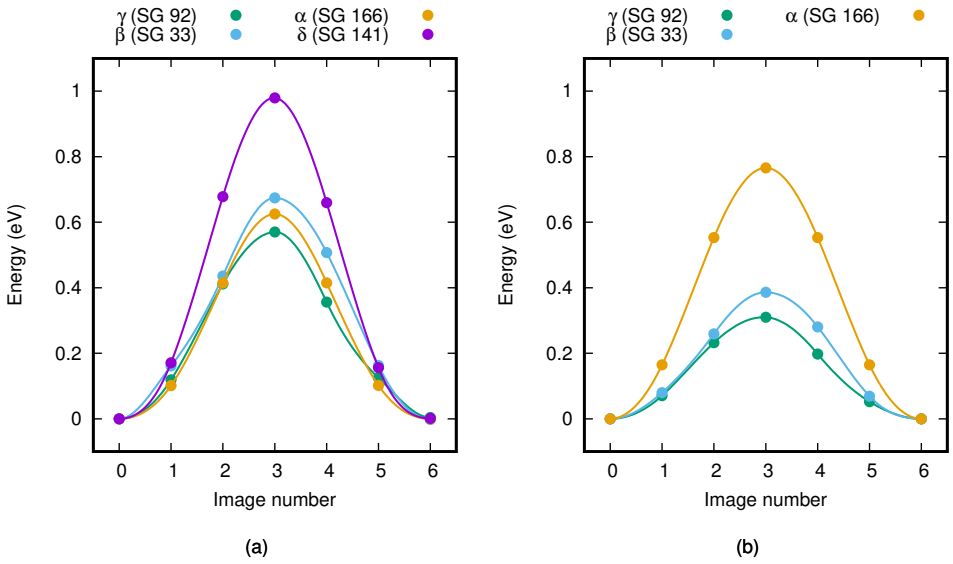

Fig. S2: Energy curve along the minimum energy path for vavancy hopping between neighbouring site in $LiAlO_2$ (a) and $NaAlO_2$.

4 Diffusion coefficient and ionic diffusivity

The *ab initio* data reported in this work can be used to estimate the diffusion coefficient and the macroscopic mobility of the charge carriers (ionic diffusivity). According to the Arrhenius equation, the diffusion coefficient can be written in terms of the activation energy E_a as

$$\mathcal{D}(T) = a^2 \nu \exp(-\beta E_\mathrm{a}) \tag{1}$$

where a is the lenght of the path, ν the attempt frequency, $\beta = (K_\mathrm{b}T)^{-1}$. Note that this is a low temperature approximation, valid as long as the enthropic contribution to the energetics is negligible. The length of the path and the activation energies are obtained as the result of a NEB calculation, whereas the attempt frequency can be identified by locating the maximum of the phonons density of state resolved on the diffusing species. Note that, given the fact the the major contribution is arising from the exponential term, it is very common in litterature to fix ν to 10 THz. In our case, we observed typical values in the range 5–6 Thz and 7–9 Thz for Na and Li atoms respectively, as can be observed in Fig. 3 in the main text. The Na atom tends to have slower oscillations, as expected from the larger mass. The values of the diffusion coefficient at room temperature are reported in Table. From these values, the macroscopic ionic conductivity can be directly calculated using the Nernst-Einstein relation

$$\sigma(T) = \frac{\mathcal{D}(T) n_\mathrm{cc} \mathrm{e}^2}{K_\mathrm{b} T} \tag{2}$$

where e is the elementary charge of an electron and n_cc the density of charge carriers. The calculated values for the γ and the α structures are reported in Table and discussed in the main text.

Table S3:

structure	a (Å)	ν (THz)	E_a (eV)	n_cc (Å^{-3})	$\mathcal{D}$ (cm^2 s^{-1})	σ (S cm^{-1})
α-$LiAlO_2$	2.83	7.0	0.62	0.030	1.87 10^{-13}	3.49 10^{-8}
γ-$LiAlO_2$	3.12	9.0	0.57	0.023	2.04 10^{-12}	2.93 10^{-7}
α-$NaAlO_2$	2.89	6.0	0.77	0.026	4.06 10^{-16}	6.58 10^{-11}
γ-$NaAlO_2$	3.26	5.0	0.31	0.020	3.07 10^{-8}	3.82 10^{-3}

5 Electronic density of states

The projected density of states (PDOS) for the examined systems are reported in Fig. 1 and in Fig. 5 for $LiAlO_2$ and $NaAlO_2$ respectively. The PDOS are normalised over the total charge per orbital type, as obtained form the Mulliken population analyses. These values are reported in the main text (Table 6). The results for the tetrahedral coordinated γ and β phases are reported in panels (a) and (c) respectively. We note that the PDOS profiles are similar, in line with the structural compatibility of these two modifications. The band gap values, reported in the main text (Table 2) are also very similar. The α and δ phases present also similar features, and the PDOS are characterised by a larger energy gap as can be appreciated from panels (b) and (d). All the examined systems present band gap values larger than 3 eV, characterising them as insulators, suitable therefore for application as electrolytes materials.

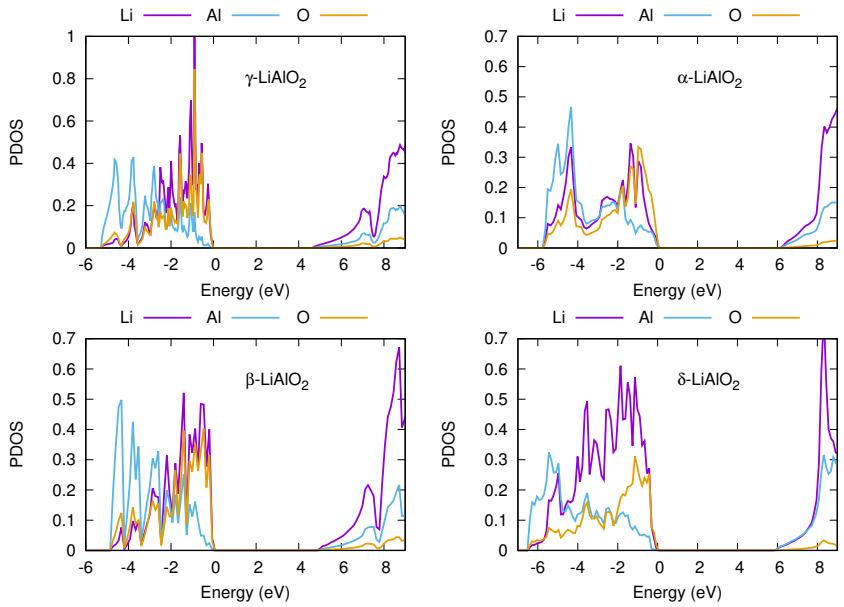

Fig. S3: Projected Density of states for the examined $LiAlO_2$ modifications. Data are normalised over the total charges as obtained by Mulliken population analysis.

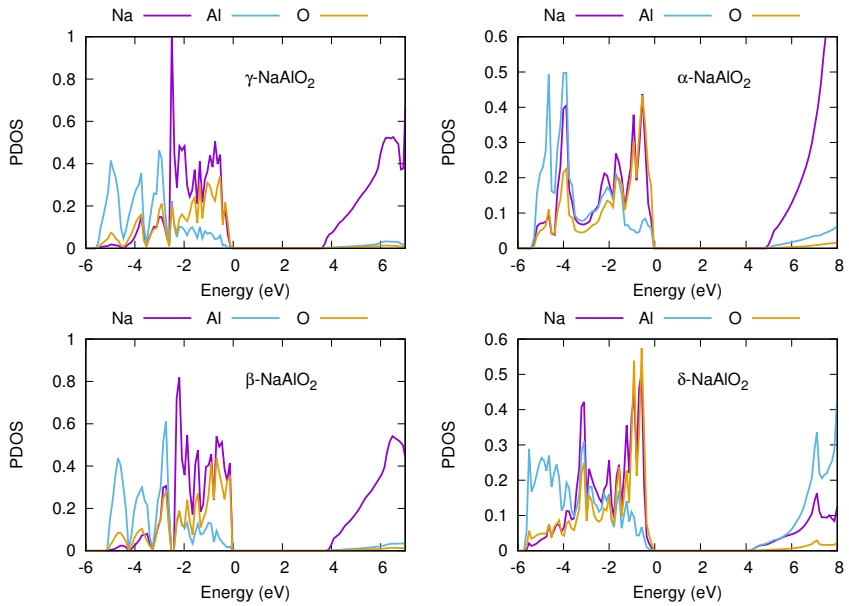

Fig. S4: Projected Density of states for the examined $NaAlO_2$ modifications. Data are normalised over the total charges as obtained by Mulliken population analysis.